Optical spectroscopic investigation of *m*-plane GaN thin films

Antaryami Mohanta,[1, 4] Yan-Zhi Tzeng,[2] Meng-En Lee,[2] Dah-Chin Ling,[3] Ying-Chieh Wang,[1] Ikai Lo,[1] and Der-Jun Jang[1,*]

[1]*Department of Physics, National Sun Yat-sen University, Kaohsiung 80424, Taiwan*
[2]*Department of Physics, National Kaohsiung Normal University, Kaohsiung 80264, Taiwan*
[3]*Department of Physics, Tamkang University, Tamsui Dist., New Taipei City 25137, Taiwan*
[4]*Current address: Department of Electrical and Computer Engineering, The University of Alabama, Tuscaloosa, Alabama 35487, USA*
**djjang@mail.nsysu.edu.tw*

Abstract: M-plane GaN thin films grown on γ-$LiAlO_2$ substrate were investigated at different temperatures by photoluminescence (PL) and time-resolved photoluminescence (TRPL) spectroscopy. The origin of two distinct emissions, P_1 and P_2 observed in the PL spectra were established by analyzing their PL and TRPL properties at different temperatures. The P_1 emission is attributed to the excitons bound to the stacking faults (SFs). The P_2 shows an anomalous "*S*-shaped" emission shift with increasing temperature (*T*), and the associated mechanism is discussed. The radiative life time 'τ_r' for P_2 emission exhibits the $T^{3/2}$ dependence at higher temperatures and deviates at lower temperatures whereas the radiative life time 'τ_r' for P_1 emission does not show the $T^{3/2}$ dependence with temperature. The polarization-dependent PL study reveals that P_2 emission involves free holes in the transition at room temperature.

©2014 Optical Society of America

OCIS codes: (250.0250) Optoelectronics; (250.5230) Photoluminescence; (300.6470) Spectroscopy, semiconductors; (300.6500) Spectroscopy, time-resolved; (310.6860) Thin films, optical properties.

References and links

1. R. Liu, A. Bell, F. A. Ponce, C. Q. Chen, J. W. Yang, and M. A. Khan, "Luminescence from stacking faults in gallium nitride," Appl. Phys. Lett. **86**(2), 021908 (2005).
2. A. Hirai, B. A. Haskell, M. B. McLaurin, F. Wu, M. C. Schmidt, K. C. Kim, T. J. Baker, S. P. DenBaars, S. Nakamura, and J. S. Speck, "Defect-mediated surface morphology of nonpolar m -plane GaN," Appl. Phys. Lett. **90**(12), 121119 (2007).
3. P. Waltereit, O. Brandt, A. Trampert, H. T. Grahn, J. Menniger, M. Ramsteiner, M. Reiche, and K. H. Ploog, "Nitride semiconductors free of electrostatic fields for efficient white light-emitting diodes," Nature **406**(6), 865–868 (2000).
4. P. P. Paskov, R. Schifano, B. Monemar, T. Paskova, S. Figge, and D. Hommel, "Emission properties of a -plane GaN grown by metal-organic chemical-vapor deposition," J. Appl. Phys. **98**(9), 093519 (2005).
5. T. Takeuchi, C. Wetzel, S. Yamaguchi, H. Sakai, H. Amano, I. Akasaki, Y. Kaneko, S. Nakagawa, Y. Yamaoka, and N. Yamada, "Determination of piezoelectric fields in strained GaInN quantum wells using the quantum-confined Stark effect," Appl. Phys. Lett. **73**(12), 1691 (1998).
6. P. Lefebvre, A. Morel, M. Gallart, T. Taliercio, J. Allègre, B. Gil, H. Mathieu, B. Damilano, N. Grandjean, and J. Massies, "High internal electric field in a graded-width InGaN/GaN quantum well: Accurate determination by time-resolved photoluminescence spectroscopy," Appl. Phys. Lett. **78**(9), 1252 (2001).
7. M. Leroux, N. Grandjean, J. Massies, B. Gil, P. Lefebvre, and P. Bigenwald, "Barrier-width dependence of group-III nitrides quantum-well transition energies," Phys. Rev. B **60**(3), 1496–1499 (1999).
8. A. Bonfiglio, M. Lomascolo, G. Traetta, R. Cingolani, A. Di Carlo, F. Della Sala, P. Lugli, A. Botchkarev, and H. Morkoc, "Well-width dependence of the ground level emission of GaN/AlGaN quantum wells," J. Appl. Phys. **87**(5), 2289 (2000).
9. D. N. Zakharov, Z. Liliental-Weber, B. Wagner, Z. J. Reitmeier, E. A. Preble, and R. F. Davis, "Structural TEM study of nonpolar *a*-plane gallium nitride grown on ($11\bar{2}0$) 4H-SiC by organometallic vapor phase epitaxy," Phys. Rev. B **71**(23), 235334 (2005).

#216506 - $15.00 USD Received 9 Jul 2014; revised 17 Aug 2014; accepted 18 Aug 2014; published 22 Aug 2014

10. W. Jian-Xia, W. Lian-Shan, Y. Shao-Yan, L. Hui-Jie, Z. Gui-Juan, Z. Heng, W. Hong-Yuan, J. Chun-Mei, Z. Qin-Sheng, and W. Zhan-Guo, "Effects of V/III ratio on *a*-plane GaN epilayers with an InGaN interlayer," Chin. Phys. B **23**(2), 026801 (2014).
11. Z. H. Wu, A. M. Fischer, F. A. Ponce, B. Bastek, J. Christen, T. Wernicke, M. Weyers, and M. Kneissl, "Structural and optical properties of nonpolar GaN thin films," Appl. Phys. Lett. **92**(17), 171904 (2008).
12. M. D. Craven, P. Waltereit, F. Wu, J. S. Speck, and S. P. DenBaars, "Characterization of *a*-plane GaN/(Al,Ga)N multiple quantum wells grown via metalorganic chemical vapor deposition," Jpn. J. Appl. Phys. **42**(2, 3A), L235–L238 (2003).
13. A. Chitnis, C. Chen, V. Adivarahan, M. Shatalov, E. Kuokstis, V. Mandavilli, J. Yang, and M. A. Khan, "Visible light-emitting diodes using a-plane GaN–InGaN multiple quantum wells over r-plane Sapphire," Appl. Phys. Lett. **84**(18), 3663 (2004).
14. A. T. Roberts, A. Mohanta, H. O. Everitt, J. H. Leach, D. Van Den Broeck, A. M. Hosalli, T. Paskova, and S. M. Bedair, "Spectroscopic investigation of coupling among asymmetric InGaN/GaN multiple quantum wells grown on non-polar a-plane GaN substrates," Appl. Phys. Lett. **103**(18), 181106 (2013).
15. C.-H. Shih, I. Lo, W.-Y. Pang, Y.-C. Wang, and M. M. C. Chou, "Characterization of M-plane GaN film grown on β-$LiGaO_2$ (100) by plasma-assisted molecular beam epitaxy," Thin Solid Films **519**(11), 3569–3572 (2011).
16. C.-H. Hsieh, I. Lo, M.-H. Gau, Y.-L. Chen, M.-C. Chou, W.-Y. Pang, Y.-I. Chang, Y.-C. Hsu, M.-W. Sham, J.-C. Chiang, and J.-K. Tsai, "Self-Assembled *c*-Plane GaN Nanopillars on γ-$LiAlO_2$ Substrate Grown by Plasma-Assisted Molecular-Beam Epitaxy," Jpn. J. Appl. Phys. **47**(2), 891–895 (2008).
17. Y. J. Sun, O. Brandt, U. Jahn, T. Y. Liu, A. Trampert, S. Cronenberg, S. Dhar, and K. H. Ploog, "Impact of nucleation conditions on the structural and optical properties of M-plane GaN (1 1 00) grown on – $LiAlO_2$," J. Appl. Phys. **92**(10), 5714 (2002).
18. L. Lymperakis and J. Neugebauer, "Large anisotropic adatom kinetics on nonpolar GaN surfaces: Consequences for surface morphologies and nanowire growth," Phys. Rev. B **79**(24), 241308 (2009).
19. W. Rieger, R. Dimitrov, D. Brunner, E. Rohrer, O. Ambacher, and M. Stutzmann, "Defect-related optical transitions in GaN," Phys. Rev. B Condens. Matter **54**(24), 17596–17602 (1996).
20. L. Eckey, J.-Ch. Holst, P. Maxim, R. Heitz, A. Hoffmann, I. Broser, B. K. Meyer, C. Wetzel, E. N. Mokhov, and P. G. Baranov, "Dynamics of bound exciton luminescences from epitaxial GaN," Appl. Phys. Lett. **68**(3), 415 (1996).
21. C. Wetzel, S. Fischer, J. Krüger, E. E. Haller, R. J. Molnar, T. D. Moustakas, E. N. Mokhov, and P. G. Baranov, "Strongly localized excitons in gallium nitride," Appl. Phys. Lett. **68**(18), 2556 (1996).
22. Z. Liliental-Weber, J. Jasinski, and D. N. Zakharov, "GaN grown in polar and non-polar directions," Opto-Electron. Rev. **12**(4), 339–346 (2004).
23. N. Nepal, J. Li, M. L. Nakarmi, J. Y. Lin, and H. X. Jiang, "Temperature and compositional dependence of the energy band gap of AlGaN alloys," Appl. Phys. Lett. **87**(24), 242104 (2005).
24. C. Stampfl and C. G. Van de Walle, "Energetics and electronic structure of stacking faults in AlN, GaN, and InN," Phys. Rev. B **57**(24), R15052–R15055 (1998).
25. M. S. Minsky, S. B. Fleischer, A. C. Abare, J. E. Bowers, E. L. Hu, S. Keller, and S. P. Denbaars, "Characterization of high-quality InGaN/GaN multiquantum wells with time-resolved photoluminescence," Appl. Phys. Lett. **72**(9), 1066 (1998).
26. L. Grenouillet, C. Bru-Chevallier, G. Guillot, P. Gilet, P. Duvaut, C. Vannuffel, A. Million, and A. Chenevas-Paule, "Evidence of strong carrier localization below 100 K in a GaInNAs/GaAs single quantum well," Appl. Phys. Lett. **76**(16), 2241 (2000).
27. A. Mohanta and R. K. Thareja, "Temperature-dependent S-shaped photoluminescence in ZnCdO alloy," J. Appl. Phys. **107**(8), 084904 (2010).
28. Z. Z. Bandic, T. C. McGill, and Z. Ikonic, "Electronic structure of GaN stacking faults," Phys. Rev. B **56**(7), 3564–3566 (1997).
29. A. Mohanta, D.-J. Jang, M.-S. Wang, and L. W. Tu, "Time-integrated photoluminescence and pump-probe reflection spectroscopy of Si doped InN thin films," J. Appl. Phys. **115**(4), 044906 (2014).
30. H.-C. Liu, C.-H. Hsu, W.-C. Chou, W.-K. Chen, and W.-H. Chang, "Recombination lifetimes in InN films studied by time-resolved excitation-correlation spectroscopy," Phys. Rev. B **80**(19), 193203 (2009).
31. J. S. Im, A. Moritz, F. Steuber, V. Härle, F. Scholz, and A. Hangleiter, "Radiative carrier lifetime, momentum matrix element, and hole effective mass in GaN," Appl. Phys. Lett. **70**(5), 631 (1997).
32. S. Ghosh, P. Waltereit, O. Brandt, H. T. Grahn, and K. H. Ploog, "Polarization-dependent spectroscopic study of M-plane GaN on γ- $LiAlO_2$," Appl. Phys. Lett. **80**(3), 413 (2002).
33. K. Domen, K. Horino, A. Kuramata, and T. Tanahashi, "Analysis of polarization anisotropy along the c axis in the photoluminescence of wurtzite GaN," Appl. Phys. Lett. **71**(14), 1996 (1997).

1. Introduction

GaN based heterostructures have been employed as potential candidates for optoelectronic devices in the ultraviolet and visible range of the electromagnetic spectrum [1]. The devices based on polar *c*-plane (0001) GaN have significant drawbacks due to the quantum confined Stark effect (QCSE) [2]. The QCSE is caused by the electrostatic fields induced due to the

spontaneous and piezoelectric polarization along the *c*-axis of GaN [3]. In group III-nitride based heterostructures grown along the *c*-axis, a strong electric field generated due to polarization discontinuities at the interfaces results in band tilting and decreases in the overlapping of the electron and hole wave functions within the quantum wells resulting in diminution in device efficiency [4]. The reduction of the oscillator strength and the redshift of the optical transitions with increasing quantum well thickness due to such built-in electric field in both InGaN/GaN and GaN/AlGaN heterostructures have been reported [5–8]. The polarization effects can be overcome if the heterostructures are fabricated in the nonpolar orientations perpendicular to the *c*-axis of GaN. Thus, the nonpolar *a*-plane and *m*-plane GaN films do not have the built-in electric field and are expected to be superior over the *c*-plane GaN thin films for high efficiency optoelectronic device fabrication. By contrast, the internal quantum efficiency of devices based on nonpolar GaN is still lower than that on polar *c*-plane GaN due to the presence of a high density of structural defects such as threading dislocations (TDs) and basal-plane stacking faults (BSFs) [1, 2, 9–11]. Therefore, an extensive investigation on the optical properties of nonpolar GaN thin layers is inevitable to realize optoelectronic devices based on nonpolar GaN. Paskov *et al*. [4] have studied the emission properties of *a*-plane GaN grown by metal-organic chemical-vapor deposition on *r*-plane sapphire and observed different emission bands in the spectral range 3.0–3.5 eV including emissions from stacking faults (SFs). GaN based *a*-plane quantum well structures grown on foreign substrates and *a*-plane GaN template have been widely investigated [12–14]. Recently, Roberts *et al*. [14] have reported spectroscopic investigations on asymmetric InGaN/GaN multiple quantum wells grown on non-polar *a*-plane GaN substrates. However, the spectroscopic investigation on *m*-plane GaN has rarely been reported in spite of the significant interest on the growth of *m*-plane GaN on different substrates by various techniques [2, 15–17]. In this paper, we have investigated in detail the *m*-plane GaN thin films grown on γ-$LiAlO_2$ substrate by photoluminescence (PL) and time-resolved photoluminescence (TRPL) at different temperatures. Two distinct emissions, P_1 and P_2 are observed in the PL spectra in which P_1 emission dominates the PL spectrum at low temperatures whereas P_2 emission dominates at higher temperatures. The P_2 emission shows an "*S*-shaped" shift with increasing temperature. The radiative life time τ_r for P_2 emission exhibits a $T^{3/2}$ dependence at higher temperatures and deviates at lower temperatures whereas the radiative life time τ_r for P_1 emission does not show the $T^{3/2}$ dependence with temperature. The polarization- dependent PL study reveals that P_2 emission involves free holes in the transition at room temperature.

2. Experimental

M-plane GaN thin films of about 1.1 µm thickness with different N/Ga flux ratios (33, 43 and 57) were grown by plasma-assisted molecular beam epitaxy on γ-$LiAlO_2$ (100) substrate. The details about the growth procedure are described elsewhere [16]. The thin films were characterized by x-ray diffraction (XRD) and scanning electron microscopy (SEM). The PL and TRPL measurements of different *m*-plane GaN thin films were performed at different temperatures using a He closed cycle cryostat. The frequency tripled output (~4.6 eV) of Ti: Sapphire laser (pulse width ~100 fs, repetition rate = 80 MHz) operating at 1.53 eV was used as the excitation source. A Si detector and standard lock-in detection technique were employed to record the PL. A time correlated single photon counting (TCSPC) detection instrument with temporal resolution of 150 ps was used to perform the TRPL experiment. The polarization-dependent PL experiment was carried out by rotating the polarization of the input laser beam with respect to the *c*-axis from $\varphi = -90°$ to 90°. The $\varphi = 0°$ (90°) corresponds to $\boldsymbol{E} \parallel c$ ($E \perp c$); where $\boldsymbol{E}$ is the electric field vector and φ is the polarization angle.

#216506 - $15.00 USD Received 9 Jul 2014; revised 17 Aug 2014; accepted 18 Aug 2014; published 22 Aug 2014

3. Results and discussion

The *m*-plane GaN thin films grown with N/Ga flux ratio of 33, 43 and 57 are designated as sample A, B and C, respectively. The XRD spectra shown in Fig. 1 have primarily two diffraction peaks corresponding to *m*-plane GaN and γ-$LiAlO_2$ substrate for all the investigated samples. The diffraction peak corresponding to *m*-plane GaN is at 32.31° for all three samples which does not show shift with N/Ga flux ratio. However, the full width at half maximum (FWHM) increases from 521 to 537 arcsec with the N/Ga flux ratio, indicating the increase of defect density with the N/Ga flux ratio.

SEM images of sample A – C are shown in Fig. 2. The density of pits and cracks observed in SEM images increases with increase in the N/Ga flux ratio *i.e.* from sample A to C which is consistent with the broadening of the diffraction line corresponding to the *m*-plane GaN indicating the increase of defect density with increase of the N/Ga flux ratio. It has been reported that the cause of these pits and cracks could be due to Ga adatom incorporation kinetics [18], and extended defects present in the form of threading dislocations (TDs) and basal-plane stacking faults (BSFs) [2].

In Fig. 3, two different emission bands named as P_1 and P_2 are observed in the PL spectra at different temperatures. The evolution of P_1 with temperature is different from that of P_2 which indicates that P_1 and P_2 are not related through phonon assisted transitions. Moreover, P_2 dominates the PL spectrum at higher temperatures; whereas P_1 dominates at lower temperatures and quenches faster than P_2 with increasing temperature. We have considered sample B with intermediate N/Ga flux ratio of 43 in this study as a representative of all samples for further analysis of the temperature dependence of P_1 and P_2. The peak energies of P_1 and P_2 at 14 K in sample B determined by curve fitting are at about 3.36 and 3.40 eV, respectively.

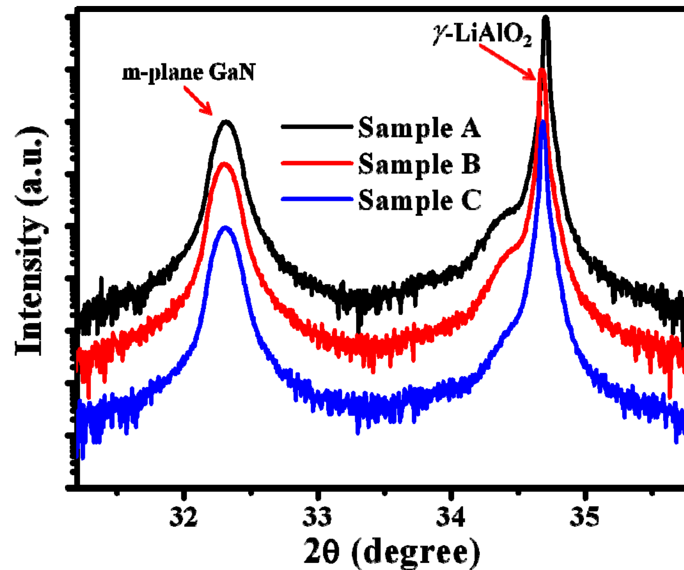

Fig. 1. XRD spectra of sample A-C contain mainly two diffraction peaks corresponding to *m*-plane GaN thin films and γ-$LiAlO_2$ substrate.

#216506 - $15.00 USD Received 9 Jul 2014; revised 17 Aug 2014; accepted 18 Aug 2014; published 22 Aug 2014

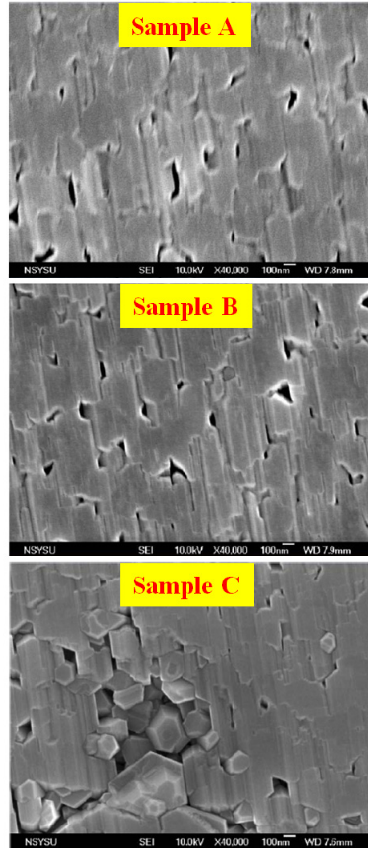

Fig. 2. SEM images of Sample A, B, and C.

As evident from Fig. 3, the intensity of the P_1 emission band increases with increasing N/Ga flux ratio *i.e.* from sample A to sample C. In addition, the temperature at which P_2 dominates P_1 is higher for higher N/Ga flux ratio i.e. at about 60 K, 80 K and 120 K for sample A, B and C, respectively. This indicates that P_1 emission could be associated with defects as defect density increases with increase of N/Ga flux ratio that is inferred from the XRD and SEM study. Note that the 3.36 eV emission has also been observed in *c*-plane GaN samples irrespective of growth techniques and has been attributed to the excitons bound to structural defects [19–21]. Furthermore, the GaN layer grown in nonpolar directions is known to have a high density of SFs [22] which play the role of luminescence centers. Liu *et al.* [1] have shown a direct correlation between the structural features associated with SFs and the emission peaks in the range of 3.29 – 3.41 eV in *a*-plane GaN epilayers. The P_1 emission at 3.36 eV appears approximately 140 meV below the band gap (E_g) of wurtzite (WZ) GaN (E_g ≈3.5 eV [23]). Investigations of the electronic structure of SFs in WZ GaN using density-functional-pseudopotential calculations reveal that no defect-induced states exist in the band gap [24]. However, SFs in GaN can form type–II quantum-well-like structures composed of very thin zinc-blende (ZB) layers embedded in the WZ host that can lead to an emission below the WZ band gap [24]. The confined electrons in the ZB quantum well layer can attract the holes through Coulomb interaction resulting in formation of excitons. The life time at 14 K obtained by fitting single exponential function to the time-resolved PL spectrum of sample B detected at 3.36 eV is about 0.7 ns, shown in Fig. 4, which is close to the value reported for the quantum wells [17, 25]. Therefore, the P_1 emission band occurring at 3.36 eV is attributed to the excitons bound to the SFs [17]. The increase in intensity of P_1 emission with increase of

#216506 - $15.00 USD Received 9 Jul 2014; revised 17 Aug 2014; accepted 18 Aug 2014; published 22 Aug 2014

N/Ga flux ratio is the signature of increasing density of SFs. The P_1 emission band shows a blueshift with increase of N/Ga flux ratio *i.e.* 3.36 eV to 3.39 eV from sample A to C, which could be associated with the different well widths of the quantum wells formed by SFs for different samples.

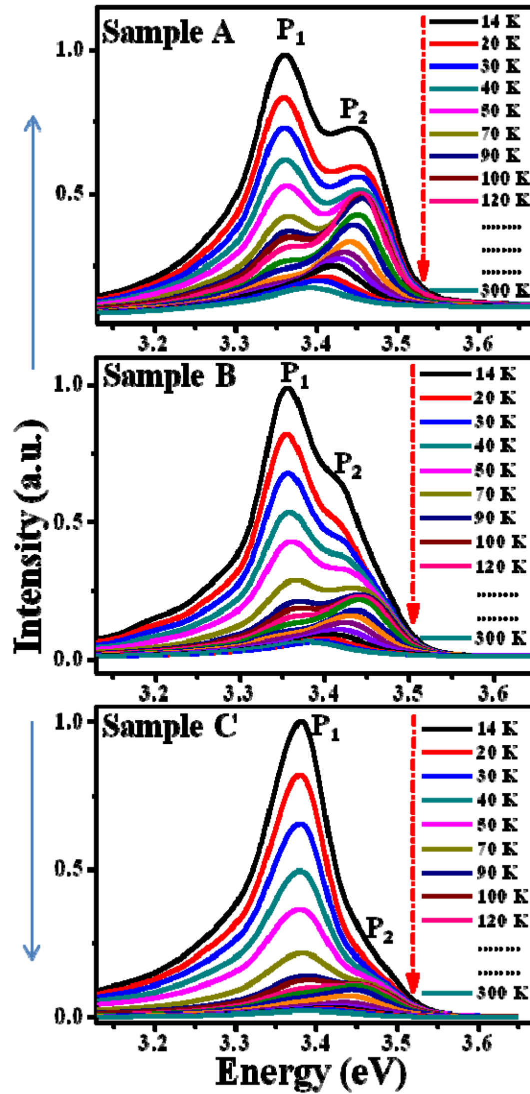

Fig. 3. PL spectra of sample A, B and C at different temperatures.

#216506 - $15.00 USD Received 9 Jul 2014; revised 17 Aug 2014; accepted 18 Aug 2014; published 22 Aug 2014

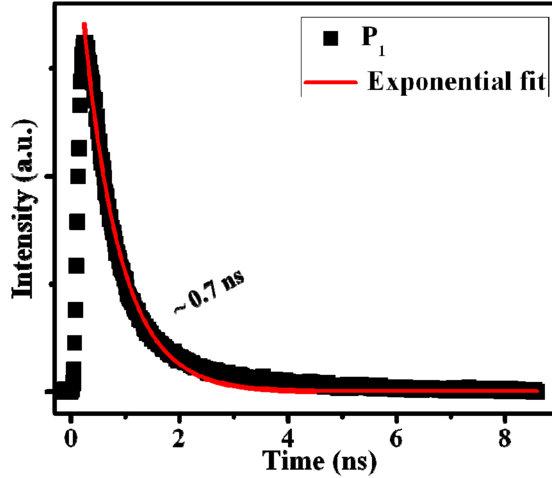

Fig. 4. TRPL spectra of sample B at 14 K detected at P_1 peak energy. The red solid line is the single exponential fit to the data points (■).

On the other hand, the peak energy of the P_2 emission band for all the samples consistently shows a blueshift at low temperatures and then evolves into a redshift at high temperatures with increasing temperature which is in strong contrast to the monotonic redshift of band gap energy predicted by Varshni's empirical formula:

$$E_g(T) = E_g(0) - \frac{\alpha T^2}{\beta + T} \tag{1}$$

It turns out that such temperature-dependent behavior is similar to the S-shaped phenomenon observed due to the presence of localized states randomly distributed in space and energy [26, 27]. The variation of peak energy of the P_2 emission band of sample B is shown in Fig. 5(a). The P_2 peak energy initially shows a blueshift with increasing temperature up to 80 K. No significant variation of P_2 peak energy is observed in the temperature range between 80 K and 120 K. Above 120 K, P_2 peak energy shows a redshift with increasing temperature. In the quantum-well-like structures with type – II band alignment formed by the SFs, electrons are deeply localized in the thin ZB quantum-well region and the holes are weakly localized in the SF electronic states originating from the heterocrystalline WZ-ZB interfaces [24, 28]. The P_2 emission could therefore be the result of such localization of carriers, and the temperature dependence of P_2 peak energy can be understood as follows. As temperature increases, localized holes are thermalized to occupy the localized states lying towards the valence band top resulting in a blueshift of P_2 emission band with an increase of temperature up to 80 K. In the temperature range between 80 K and 120 K, the blueshift due to the thermalization of localized holes is compensated by the redshift arising from temperature-induced band gap shrinkage. Above 120 K, the temperature-induced band gap shrinkage dominates and gives rise to the redshift of the P_2 peak energy with increasing temperature. The theoretical curve represented by the red dashed line in Fig. 5(a) is obtained using Eq. (1), indicating that the P_2 peak energy above 120 K follows Varshni's empirical formula. Similar temperature dependence of P_2 peak energy is also observed for sample A and C, respectively.

#216506 - $15.00 USD Received 9 Jul 2014; revised 17 Aug 2014; accepted 18 Aug 2014; published 22 Aug 2014

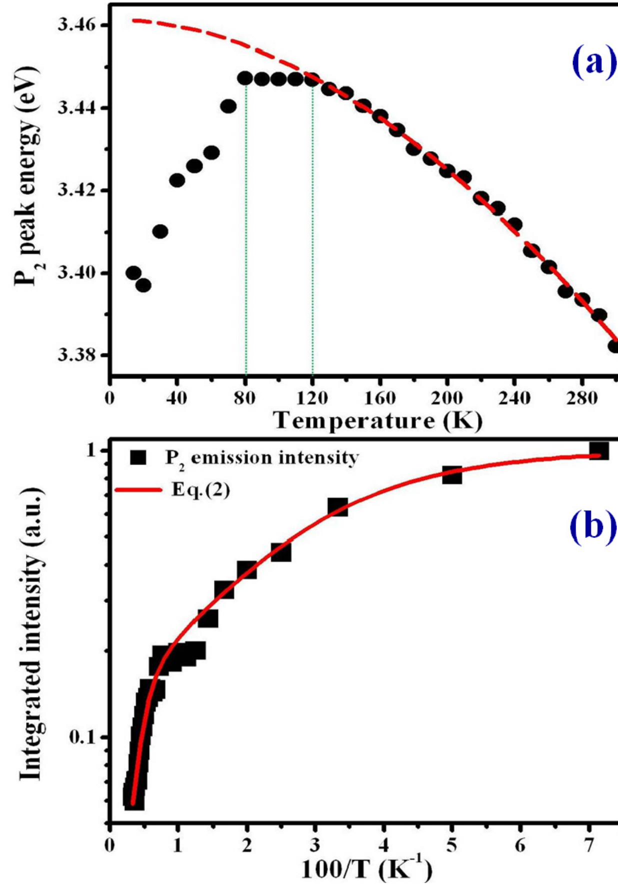

Fig. 5. (a) Temperature dependence of peak energy of P_2 emission band of sample B is represented by solid circle (●). The dashed line is a theoretical curve obtained from Varshni's empirical formula. The two vertical dotted lines represent the data points at 80 and 120 K respectively. (b) Temperature dependence of integrated intensity of P_2 emission band is represented by the solid squares (■). The solid line is the theoretical fit using Eq. (2).

The temperature dependence of the integrated intensity of P_2 emission band shown in Fig. 5(b) is analyzed in order to further understand the thermalization of localized electrons and holes. The integrated intensity of the P_2 emission band is estimated by using curve fitting. The decrease of intensity with an increase of temperature is due to the thermal quenching process. The solid line is the theoretical fit to the data points using the following relation that is comprised of two nonradiative channels [29]:

$$I(T) = \frac{I_0}{\left[1 + a_1 \exp\left(-\frac{E_1}{k_B T}\right) + a_2 \exp\left(-\frac{E_2}{k_B T}\right)\right]} \tag{2}$$

where $I(T)$ and I_0 are the integrated PL intensities at temperature T and 0 K, respectively. The coefficients a_1 and a_2 are the measure of the strengths of both the thermal quenching processes. E_1 and E_2 are the activation energies at low temperature and high temperature regions, respectively. The fitting using Eq. (2) to the data points shown in Fig. 5(b) gives E_1 = 6.3 meV and E_2 = 68 meV, respectively. The activation energy E_1 (6.3 meV) in the low temperature region corresponds to about 74 K, indicative of the delocalization of holes above 74 K. It can account for the suppression of the blueshift of P_2 peak energy above 80 K as

#216506 - $15.00 USD Received 9 Jul 2014; revised 17 Aug 2014; accepted 18 Aug 2014; published 22 Aug 2014

shown in Fig. 5(a). The activation energy E_2 = 68 meV in the high temperature region could correspond to the delocalization of electrons from the ZB quantum well region formed by SFs. The P_2 emission at higher temperatures after the delocalization of holes could be attributed to a recombination of localized excitons or a recombination between electrons localized in the ZB quantum well region and free holes in the valence band [4].

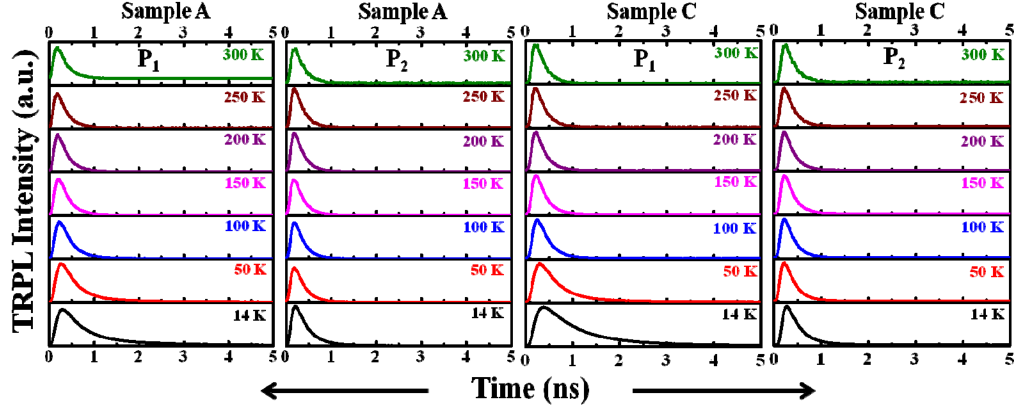

Fig. 6. TRPL spectra at different temperatures of sample A and C detected at P_1 and P_2 peak energies.

The time-resolved PL spectra of sample A and C having low and high N/Ga flux ratios respectively are shown in Fig. 6. The decay times are obtained by fitting the PL decay curves using single exponential function, $I(t) = I(0)\exp\left(-\frac{t}{\tau}\right)$; where τ is the decay time. The decay times for P_1 and P_2 are shown in Fig. 7 at different temperatures. At low temperatures, the recombination process is mostly radiative in nature. In order to have clear insight on the P_1 and P_2 emissions, radiative lifetime (τ_r) is extracted from the decay time τ by using the following relations:

$$\tau_r = \frac{\tau}{\eta} \tag{3}$$

where η is the quantum efficiency. The ratio of integrated PL intensity at temperature T to that at 14 K can be used as a measure for quantum efficiency by assuming that the nonradiative channels are inactive at the lowest temperature. The radiative life times at P_1 and P_2 peak energies for sample A and C are shown at different temperatures in Fig. 7. The radiative lifetime varies with temperature as $\tau_r \sim T^{3/2}$ for radiative band to band recombination [30, 31]. The solid line represents $\tau_r \sim T^{3/2}$ fit to the data points. The radiative life time τ_r for P_1 does not follow a $\tau_r \sim T^{3/2}$ dependence with temperature for all three samples, whereas the radiative life time τ_r for P_2 exhibits the $T^{3/2}$ dependence at higher temperatures. These experimental findings indicate that P_2 emission involves excitons or free carrier recombination at higher temperatures [31] which is consistent with the redshift behavior of P_2 peak energy with temperature in accordance with Varshni's formula [Fig. 5(a)]. At low temperatures, the variation of radiative life time of P_2 with temperature deviates from a $\tau_r \sim T^{3/2}$ dependence that could be attributed to the localization of holes in the SF electronic states originating from the heterocrystalline WZ-ZB interfaces [24, 28, 30]. Moreover, the deviation of the temperature dependence of radiative life time of P_1 from $\tau_r \sim T^{3/2}$ behavior supports the origin of P_1 emission due to excitons bound to SFs [17, 30].

#216506 - $15.00 USD Received 9 Jul 2014; revised 17 Aug 2014; accepted 18 Aug 2014; published 22 Aug 2014

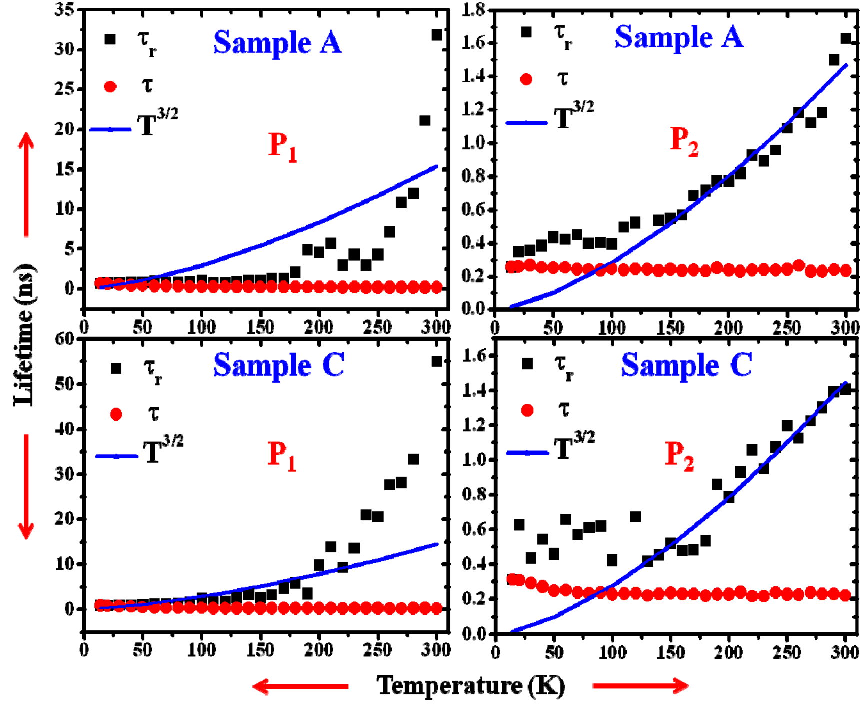

Fig. 7. Variation of τ and τ_r at P_1 and P_2 peak energies of sample A and C with temperature is represented by the solid circles (●) and squares (■), respectively. The solid line represents the $T^{3/2}$ fit to the data points.

In *m*-plane GaN thin films, the unique *c*-axis of WZ GaN lies in the growth plane that results in an optical anisotropy for the light electric-field vector (***E***) polarized parallel (||) and perpendicular (⊥) to the *c*-axis [32]. The PL spectra of sample A recorded at different polarization angle φ (φ = 0° or 90° refers to $\boldsymbol{E}\parallel c$ or $\boldsymbol{E}\perp c$) at room temperature is shown in Fig. 8(a). The integrated PL intensity and the PL peak energy at different angle 'φ' are shown in Fig. 8(b). The integrated intensity is minimum for $\boldsymbol{E}\parallel c$ and is maximum for $\boldsymbol{E}\perp c$.

The polarization ratio 'ρ' is defined as:

$$\rho = \frac{I_{E\perp c} - I_{E\parallel c}}{I_{E\perp c} + I_{E\parallel c}} \tag{5}$$

where $I_{E\perp c}$ and $I_{E\parallel c}$ are the PL intensities for $\boldsymbol{E}\perp c$ and $\boldsymbol{E}\parallel c$, respectively, and is estimated to be ρ ~58%. Furthermore, the PL peak energy increases as the polarization angle φ changes from 0° to 90° or −90° *i.e.* from $\boldsymbol{E}\parallel c$ to $\boldsymbol{E}\perp c$. This can be understood by considering the electronic band structure in WZ GaN which has three closely spaced top valence bands (VBs) at the Brillouin-zone center (BZC): (i) heavy hole (HH) [Γ_9], (ii) Light hole (LH) [upper Γ_7] and (iii) crystal field split-off hole (CH) [lower Γ_7]. For $\boldsymbol{E}\perp c$, the transition dominantly involves the HH and LH band whereas the transition involves dominantly the CH band for $\boldsymbol{E}\parallel c$ [32]. Therefore, the PL peak energy for $\boldsymbol{E}\parallel c$ (φ = 0°) is higher than that for $\boldsymbol{E}\perp c$ (φ = 90°) as shown in Fig. 8(b). In addition, the PL intensity for $\boldsymbol{E}\parallel c$ (φ = 0°) is lower because of the smaller thermal distribution of carriers for the CH band [33]. Similar polarization-dependent behavior has been observed for samples B and C. The polarization-dependent PL study discussed above reveals that the P_2 emission involves free holes in the transition at room temperature since PL at room temperature is predominantly the P_2 emission.

#216506 - $15.00 USD Received 9 Jul 2014; revised 17 Aug 2014; accepted 18 Aug 2014; published 22 Aug 2014

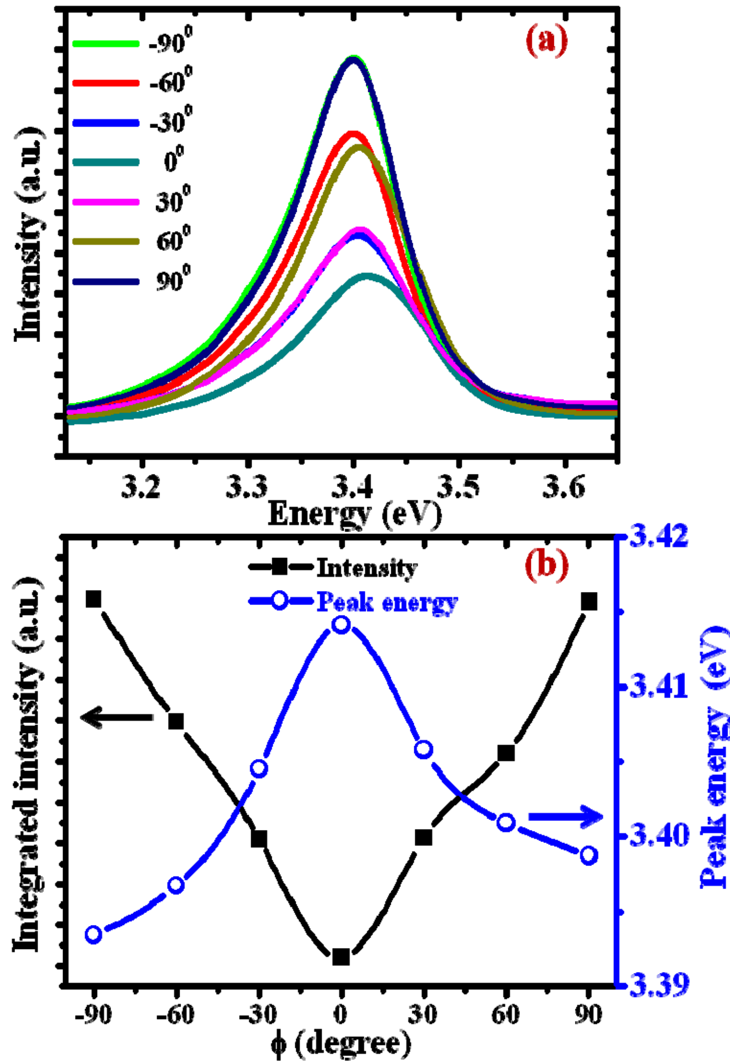

Fig. 8. (a) PL spectra of sample A at different polarization angles (φ) at room temperature. (b) Variation of integrated PL intensity and PL peak energy of sample A with polarization angle φ at room temperature.

4. Conclusions

In summary, the m-plane GaN thin films grown by plasma-assisted molecular beam epitaxy with different N/Ga flux ratios are investigated. The PL spectra contain two distinct emissions: P_1 and P_2. The P_1 emission increases its intensity with N/Ga flux ratio and is attributed to the excitons bound to the SFs. The P_2 shows an anomalous "S-shaped" emission shift with an increase of temperature. As the temperature increases, localized holes are thermalized to occupy the localized states lying towards the valence band top resulting in a blueshift of the P_2 emission band with an increase of temperature up to 80 K. In the temperature range between 80 K and 120 K, the blueshift due to the thermalization of localized holes is compensated by the redshift arising from temperature-induced band gap shrinkage. Above 120 K, the temperature-induced band gap shrinkage dominates and gives rise to the redshift of the P_2 peak energy with increasing temperature. The radiative life time as a function of temperature for P_1 emission does not follow the $T^{3/2}$ dependence which

#216506 - $15.00 USD Received 9 Jul 2014; revised 17 Aug 2014; accepted 18 Aug 2014; published 22 Aug 2014

supports the origin of P_1 emission due to excitons bound to SFs. On the other hand, the radiative life time for P_2 emission exhibits the $T^{3/2}$ dependence at higher temperatures and deviates at lower temperatures. This indicates that P_2 emission involves excitons or free carrier recombination at higher temperatures which is consistent with the redshift behavior of P_2 peak energy with temperature in accordance with Varshni's formula. Furthermore, the polarization-dependent PL study reveals that P_2 emission involves free holes in the transition at room temperature.

Acknowledgment

This research was supported by the National Science Council of the Republic of China under Grant No. NSC 101-2112-M-110-011.

#216506 - $15.00 USD   Received 9 Jul 2014; revised 17 Aug 2014; accepted 18 Aug 2014; published 22 Aug 2014